

Multifractal behavior of linear polymers in disordered media

Anke Ordemann,^{1,2} Markus Porto,³ H. Eduardo Roman,⁴ Shlomo Havlin,^{2,1} and Armin Bunde¹

¹*Institut für Theoretische Physik III, Justus-Liebig-Universität Giessen, Heinrich-Buff-Ring 16, 35392 Giessen, Germany*

²*Minerva Center and Department of Physics, Bar-Ilan University, 52900 Ramat-Gan, Israel*

³*School of Chemistry, Tel Aviv University, 69978 Tel Aviv, Israel*

⁴*INFN, Sezione di Milano, Via Celoria 16, 20133 Milano, Italy*

(Received 7 January 2000)

The scaling behavior of linear polymers in disordered media modeled by self-avoiding random walks (SAWs) on the backbone of two- and three-dimensional percolation clusters at their critical concentrations p_c is studied. All possible SAW configurations of N steps on a single backbone configuration are enumerated exactly. We find that the moments of order q of the total number of SAWs obtained by averaging over many backbone configurations display multifractal behavior; i.e., different moments are dominated by different subsets of the backbone. This leads to generalized coordination numbers μ_q and enhancement exponents γ_q , which depend on q . Our numerical results suggest that the relation $\mu_1 = p_c \mu$ between the first moment μ_1 and its regular lattice counterpart μ is valid.

PACS number(s): 61.41.+e, 05.40.-a, 61.43.-j

I. INTRODUCTION

The question of how linear polymers behave in a disordered medium has attracted much attention in recent years. The problem is not only interesting from a theoretical point of view, but may also be relevant for understanding transport properties of polymeric chains in porous media, such as enhanced oil recovery, gel electrophoresis, gel permeation chromatography, etc. [1–4]. In this context, it is useful to learn about the static or conformational properties of linear chains, modeled by self-avoiding walks (SAWs), in the presence of quenched disorder, e.g., how the surrounding structural disorder influences their spatial configuration. As a quite general model of a random medium, percolation [5–8] may be considered the paradigm for a broad class of disordered systems and has therefore been mostly used so far.

We are interested in how the statistical behavior of SAWs on percolation clusters at criticality ($p = p_c$) differs from their behavior on regular lattices. While the values of the exponents for SAWs on regular lattices are well established [1,9–12], there is no complete agreement about their values on percolation clusters at p_c [13,14]. Here we study (i) the so-called effective coordination number of the cluster, where contradicting results have been reported using different numerical techniques. Next we consider (ii) the enhancement exponent γ and (iii) the exponents ν_r and ν_l , characterizing the end-to-end distance of SAWs in the r - and l -space metrics. Finally, we determine (iv) the values of the critical exponents describing the corresponding structural distribution functions.

We concentrate on SAWs on percolation clusters at p_c in two and three dimensions. In the literature, two distinct methods have been used for evaluating SAWs: Exact enumeration (EE) and Monte Carlo (MC) simulation. In the EE technique, *all* SAW configurations on a given cluster are taken into account, but only relatively short chains can be evaluated. In a MC simulation, longer chains can be studied, but inherently the ensemble of configurations remains incomplete. Here we use the EE technique in combination with

an appropriate finite-size scaling procedure to determine the relevant exponents. Since ‘‘infinitely’’ long chains can only exist on the backbone of the cluster, where dangling ends are absent on all length scales, we study the SAWs directly on the backbone. This enables us to generate longer chains on a given cluster and to average over a larger set of different cluster configurations.

Specifically, we enumerate all possible SAW configurations of N steps for a single backbone and study different moments of the total number of SAWs and their end-to-end distance by averaging over many different backbone configurations. Our analysis shows that the critical exponents ν_r and ν_l do not depend on the order q of the moments, while the enhancement exponents and the effective coordination numbers do depend on q , leading to multifractal behavior. In particular, we find that the first moment of the effective coordination number μ_1 satisfies $\mu_1 = p_c \mu$, where μ is the effective coordination number of the underlying regular lattice, resolving previous controversies. The mean structural distribution functions for the end-to-end distance after N steps, both in Euclidean and topological space, are obtained numerically, supporting the expected scaling forms [15,16].

The paper is organized as follows: In Sec. II, we briefly review the main relevant properties of SAWs on regular lattices to illustrate the different numerical procedures employed in this work. In Sec. III, we present results for the total number and the mean end-to-end distance of SAWs on the backbone of the incipient percolation cluster. The corresponding distribution functions of the end-to-end distance and their scaling behavior, in Euclidean and topological space, are also discussed. Finally, in Sec. IV we summarize our main results.

II. SAWS ON REGULAR LATTICES REVIEWED

In this section, we illustrate the different numerical techniques we use in the following sections by briefly reviewing the main results for SAWs on regular lattices. The main idea is to show that our finite-size scaling, employed in the later

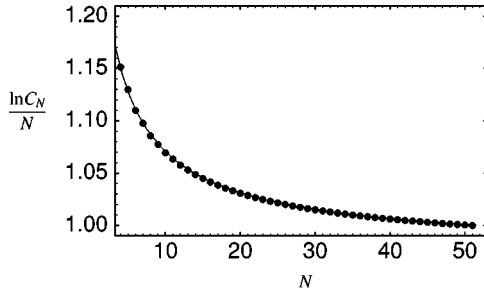


FIG. 1. The total number C_N of SAW configurations on the square lattice plotted as $(\ln C_N)/N$ versus N , from the presently available exact enumeration results for C_N , $N \leq 51$ [17]. The continuous line corresponds to a numerical fit obtained in the range $10 \leq N \leq 51$ using Eq. (2), with $\mu = 2.641$, $\gamma = 1.3$, and $A = 1.35$.

sections, enables us to obtain quite accurate estimates for the critical exponents based on EE results for relatively short chains. Here we consider the case $d=2$, which is particularly suitable since many results are known exactly.

A. Total number of SAW configurations C_N

The total number C_N of SAW configurations of N steps behaves as [11]

$$C_N = A \mu^N N^{\gamma-1}, \quad (1)$$

where μ is the effective coordination number of the lattice, γ is the universal enhancement exponent, and A is a constant. To determine μ , γ , and A , we choose to study the behavior of the quantity

$$\frac{\ln C_N}{N} = \frac{\ln A}{N} + \ln \mu + (\gamma - 1) \frac{\ln N}{N} \quad (2)$$

as a function of N . Figure 1 shows that for the square lattice, the values for μ and γ obtained by fitting the EE data using Eq. (2) agree well with the accepted values reported in the literature (see Table I).

B. Mean end-to-end distance and structural distribution function

The root mean-square end-to-end distance of SAWs of N steps, $\bar{r}(N) \equiv [r^2(N)]^{1/2}$, averaged over all possible SAW configurations behaves as

TABLE I. Structural parameters for SAWs on regular lattices in $d=2$. Results of the present simulations obtained on the square lattice, compared with the accepted values from the literature.

	Literature	Present results
λ	43/32 ^a	1.30 ± 0.05
μ	2.6385 ± 0.0001 ^b	2.641 ± 0.005
ν_F	3/4 ^c	0.745 ± 0.005
g_1	11/24 ^d	0.4 ± 0.1
g_2	5/8 ^e	0.61 ± 0.05
δ	4 ^f	4.5 ± 0.5

^aReference [18].

^dReference [21].

^bReferences [19,20].

^eReference [22].

^cReference [9].

^fReference [10].

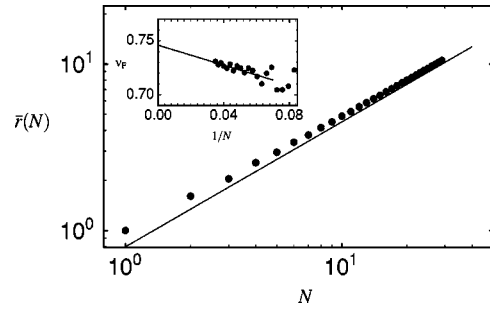


FIG. 2. The mean end-to-end distance $\bar{r}(N)$ versus N for SAWs on the square lattice. The continuous line is drawn as a guide and its slope has the theoretical value $\nu_F = 3/4$. In the inset, the successive slopes $\nu_F = d \ln \bar{r}(N) / d \ln N$ are plotted versus $1/N$. A linear extrapolation of the points to the limit $1/N \rightarrow 0$ yields our estimate $\nu_F = 0.745 \pm 0.005$, consistent with the value $3/4$.

$$\bar{r}(N) \propto N^{\nu_F}, \quad (3)$$

with the universal exponent $\nu_F = 3/4$ in $d=2$ as suggested by Flory [9]. In Fig. 2, we show values for $\bar{r}(N)$ versus N obtained by the EE technique [17]. The asymptotic value for ν_F (see also Table I) is obtained using successive slopes, as shown in the inset of Fig. 2, and is in excellent agreement with the theoretical prediction.

More detailed information about the spatial structure of SAWs is given by the distribution function $P(r, N)$, where $P(r, N) dr$ is the probability that after N steps, the end-to-end distance of a chain is between r and $r + dr$. This quantity obeys the scaling form [11,12]

$$P(r, N) \propto \frac{1}{r} f(r/N^{\nu_F}) \quad (4)$$

and is normalized according to $\int_0^\infty dr P(r, N) = 1$. The analytic form of the scaling function $f(x)$ is known asymptotically:

$$f(x) \propto \begin{cases} x^{g_1+d}, & x \leq 1 \\ x^{g_2+d} \exp(-cx^\delta), & x \gg 1, \end{cases} \quad (5)$$

where $g_1 = (\gamma - 1) / \nu_F$ [21], $g_2 = \delta(d(\nu_F - 1/2) - (\gamma - 1))$ [22], and $\delta = 1/(1 - \nu_F)$ [10]. Values for these exponents are summarized in Table I. We have verified these predictions by enumerating all SAW configurations for $N=23$ and 24 and calculating the corresponding distributions $P(r, N)$, from which we have extracted the different exponents (see Fig. 3). We show that a more accurate determination of the exponent g_2 compared to a simple fit using Eq. (5) can be obtained by employing a specific numerical procedure described in Appendix A (see inset of Fig. 3). The obtained values are in agreement with the theoretical predictions (see Table I).

III. SAWS ON THE BACKBONE OF THE INCIPIENT PERCOLATION CLUSTER

Next, we consider SAWs on the incipient percolation cluster by generating all SAW configurations directly on the backbone of the cluster. We obtain the backbone of a given cluster grown by the Leath algorithm [23,24] by randomly

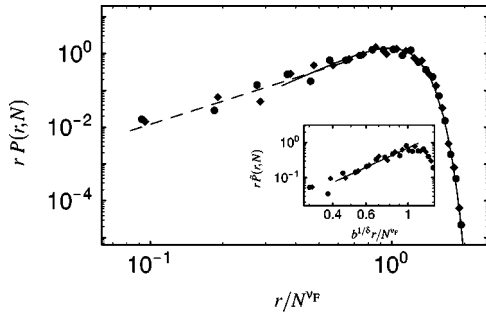


FIG. 3. The structural distribution function of SAWs, $rP(r,N)$ versus r/N^{ν_F} with $\nu_F=3/4$, for $N=23$ (diamonds) and $N=24$ (circles) on the square lattice. The dashed line in the range $r/N^{\nu_F} < 1$ has a slope $g_1+d=2.4$, and the one for $r/N^{\nu_F} > 1$ is a fit with Eq. (5), for $x \gg 1$, yielding $g_2+d=2.9 \pm 0.4$, $\delta=4.5 \pm 0.8$, and $c=0.7 \pm 0.1$. In the inset, we show the function $r\tilde{P}(r,N) \equiv b^{(g_2+d)/\delta}(\Omega B)^{-1}rP(r,N)\exp[(b^{1/\delta}r/N^{\nu_F})^\delta] = b(r/N^{\nu_F})^\delta$ versus $b^{1/\delta}r/N^{\nu_F}$, following the procedure described in Appendix A, allowing a more precise determination of g_2 . For our estimate of the crossover value $z=0.4$, the continuous line has a slope $g_2+d=2.61 \pm 0.05$, in agreement with the theoretical value (see Table I).

choosing *one* of the sites of the last grown cluster shell (e.g., site A in Fig. 4) and determining the backbone between site A and the seed of the cluster (site S in Fig. 4) by the burning procedure described in [25,26]. The SAWs start at the seed S of the cluster. To avoid finite size effects, the chemical distance between both end points S and A of the backbone is chosen to be at least 20 times larger than the chemical length of the SAWs. The large ratio between both chemical lengths is needed, since close to the end point A , the backbone has a quasilinear structure, which would falsify the results for the SAWs. The straightforward idea to use *all* sites on the last grown shell as end points for the backbone does not help, but introduces boundary effects in the opposite direction, since in this case the backbone coincides with the cluster near the end points; cf. [26].

We analyze the results for SAWs on the incipient percolation cluster by applying analogous numerical procedures on the data as described above for SAWs on regular lattices. In contrast to the case of regular lattices, on a percolation cluster two different metrics can be defined: the Euclidean metric and the topological or chemical metric. On average,

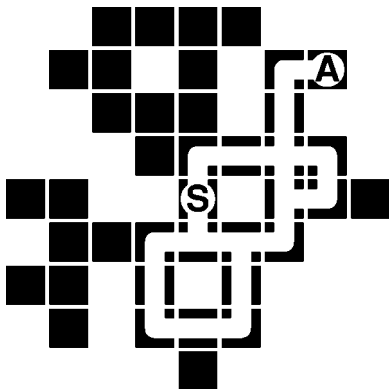


FIG. 4. A percolation cluster on the square lattice (full squares) and its corresponding backbone between the seed S and a site A randomly chosen on the last grown shell.

the chemical distance l between two backbone sites separated by the Euclidean distance r increases with r as [27,28]

$$l \propto r^{d_{\min}}, \quad (6)$$

where $d_{\min}=1.1306 \pm 0.0003$ in $d=2$ [29] and $d_{\min}=1.374 \pm 0.004$ in $d=3$ [30]. Thus Eq. (6) yields the scaling relation between the two metrics, which will be used in what follows. Numerically it is found that data obtained in l space show less fluctuations (cf., e.g., [15]). Therefore more accurate estimates for many characteristic quantities (such as critical exponents) in r space can be determined by studying the corresponding quantity in l space and transforming it to r space. For example, the fractal dimension of the backbone in l space is $d_l^B=1.45 \pm 0.01$ in $d=2$ and $d_l^B=1.36 \pm 0.02$ in $d=3$. Using Eq. (6), this leads to the values $d_f^B=d_l^B d_{\min}=1.64 \pm 0.02$ and $d_f^B=1.87 \pm 0.03$ in r space, respectively [26].

A. Total number of SAW configurations: Multifractality

Due to the disordered structure of the clusters, the total number $C_{N,B}$ of SAW configurations that are generated on a single backbone, with the seed S of the cluster as the starting point, fluctuates strongly among different backbone configurations. To characterize these fluctuations, we study the moments $\langle C_{N,B}^q \rangle$. A similar study on percolation clusters at criticality has been performed for “ideal” chains; i.e., chains that can intersect themselves. This model leads to a non-trivial dependence on q [31].

In generalizing Eq. (1), we make the ansatz

$$\langle C_{N,B}^q \rangle^{1/q} = A_q \mu_q^N N^{\gamma_q - 1}, \quad (7)$$

where μ_q are the generalized effective coordination numbers of the backbone and γ_q the generalized enhancement exponents. Results for different values of q are shown in Figs. 5(a) and 5(b) for the square and simple cubic lattice, respectively, employing the numerical procedure described in Sec. II A. The values for μ_q and γ_q are displayed in Fig. 6 for $d=2$, clearly revealing a dependence on q , reminiscent of a multifractal behavior. For large negative values of q , backbone configurations with a small number of SAW configurations $C_{N,B}$ are singled out in the averaging procedure. We find that $\mu_q \rightarrow 1$ and $\gamma_q \rightarrow 1$ for $q \rightarrow -\infty$, pointing to rare configurations of backbones with an almost linear shape. On the contrary, for large values of q the averaging procedure emphasizes backbone configurations with a large number of SAW configurations $C_{N,B}$. Since these backbones are the most compact ones, μ_q and γ_q are strongly enlarged. Figure 6 seems to suggest that the structure of the most compact backbone differs distinctively from the structure of a regular square lattice, as $\lim_{q \rightarrow \infty} \mu_q \approx 1.9$, which is well below the value for μ on the regular square lattice, and $\lim_{q \rightarrow \infty} \gamma_q \approx 1.7$ is well above the value for γ on the regular square lattice.

These results resolve earlier controversies regarding the values for both μ and γ for percolation obtained from MC simulations and by EE techniques. For the square lattice, for example, the values $\mu_{\text{perc}}(\text{EE})=1.53 \pm 0.05$ [32] and $\gamma_{\text{perc}}(\text{EE})=1.33 \pm 0.02$ [33] have been obtained from exact enumeration calculations, while from MC simulations the

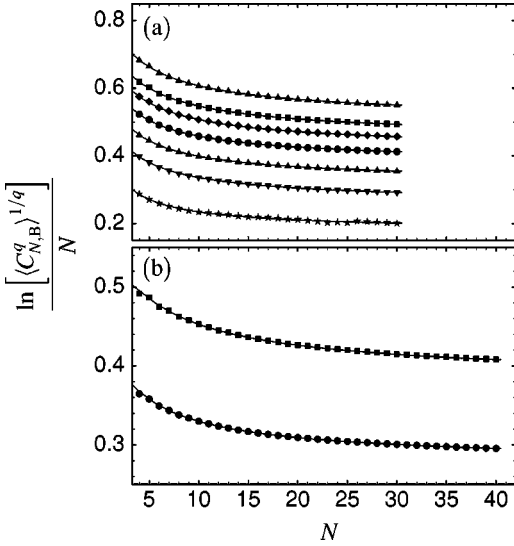


FIG. 5. Generalized moments $\langle C_{N,B}^q \rangle$ of the total number $C_{N,B}$ of SAW configurations on the backbone of critical percolation clusters, plotted as $(1/N)\ln[\langle C_{N,B}^q \rangle^{1/q}]$ versus N . (a) On the square lattice, for $q=2, 1, 0.5, 0, -0.5, -1$, and -2 (from top to bottom); (b) on the simple cubic lattice, for $q=1$ (top) and $q=0$ (bottom). Averages over 10^5 backbone configurations each are performed. The continuous lines are the best fits based on Eq. (7), yielding the values for μ_q and γ_q for $q=0$ and 1 given in Table II. Some representative values for γ_q , in addition to those reported in Table II, are $\gamma_{-2}=1.15\pm 0.05$, $\gamma_{-1}=1.23\pm 0.05$, and $\gamma_2=1.36\pm 0.05$ in $d=2$. Values of A_q are found to fluctuate in the range 1.0–1.3 in both $d=2$ and $d=3$.

values $\mu_{\text{perc}}(\text{MC})=1.459\pm 0.003$ and $\gamma_{\text{perc}}(\text{MC})=1.31\pm 0.03$ [34] were determined. We find $\mu_1=1.565\pm 0.005$, $\gamma_1=1.34\pm 0.05$, and $\mu_0=1.456\pm 0.005$, $\gamma_0=1.26\pm 0.05$, corresponding to the EE and MC results, respectively. This can be understood by noting that EE calculations yield by definition the whole ensemble (the so-called “annealed” average), corresponding to the case $q=1$; i.e., the normal arithmetic average. In contrast, MC simulations intrinsically sample only a small subset of all possible configurations, omitting rare configurations, yielding “typical” subsets of

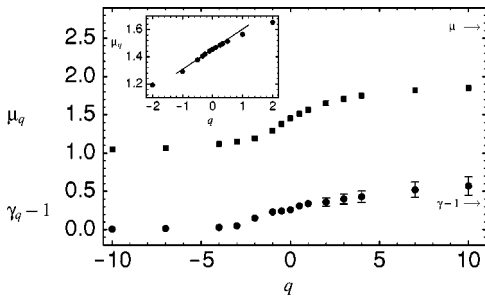


FIG. 6. The effective coordination numbers μ_q and enhancement exponents γ_q versus q for $-10\leq q\leq 10$ in $d=2$ obtained from Fig. 5(a). Expect for γ_q for $q\geq 2$, the error bars are smaller than the symbol sizes. The values for μ and γ on regular square lattice are marked by arrows, clearly showing that $\lim_{q\rightarrow\infty}\gamma_q$ is larger than γ on regular square lattice. The inset shows μ_q versus q for $-2\leq q\leq 2$ in $d=2$, in good agreement with the theoretical result $\mu_q=\mu_0(1+q\sigma_0^2/2)$ (continuous line) expected for $|q|\rightarrow 0$ [16], with $\mu_0=1.456$ and $\sigma_0=0.45$.

the ensemble (the so-called “quenched” average). This quenched average is usually described by a logarithmic average, i.e., $\langle C_{N,B} \rangle_{\text{typ}} \equiv \exp\langle \ln C_{N,B} \rangle$, and is equivalent to the limit $q\rightarrow 0$ of Eq. (7); i.e., $\lim_{q\rightarrow 0}\langle C_{N,B}^q \rangle^{1/q} = \exp\langle \ln C_{N,B} \rangle$. Indeed, our results are in excellent agreement, in both $d=2$ and $d=3$, with the relation

$$\mu_1 = p_c \mu, \quad (8)$$

where μ is the effective coordination number of the underlying regular lattice, $p_c=0.5927460$ for the square lattice [35] and $p_c=0.311605$ for the simple cubic lattice [36]. This relation, which was originally suggested in the form $\mu_{\text{perc}} = p_c \mu$ [34], could not be confirmed earlier on because of the different values obtained for μ_{perc} . Because of the possible existence of rare events playing a dominant role in the average procedure, we have performed a detailed analysis of our numerical data to confirm that we have considered a sufficiently large set of cluster configurations (cf. Appendix B).

B. Mean end-to-end distances and structural distribution functions

Next we study the scaling behavior of the distribution functions for the end-to-end distance, $\langle P_B(l, N) \rangle$ and $\langle P_B(r, N) \rangle$, averaged over many backbone configurations, where $P_B(l, N)dl$ is the probability that after N steps, the chemical end-to-end distance of a chain on a single backbone is between l and $l+dl$, and $P_B(r, N)dr$ is the analogous quantity in r space. These distribution functions are expected to obey scaling forms similar to the one valid on regular lattices, Eq. (4), with the corresponding scaling exponents [15]. The mean chemical end-to-end distance $\langle \bar{l}(N) \rangle$ and the root mean-square Euclidean end-to-end distance $\langle \bar{r}(N) \rangle \equiv \langle [r^2(N)]^{1/2} \rangle$ scale with N as

$$\langle \bar{l}(N) \rangle \propto N^{\nu_l}, \quad (9)$$

$$\langle \bar{r}(N) \rangle \propto N^{\nu_r}, \quad (10)$$

respectively. The first average is performed over all SAW configurations on a single backbone; the second average is carried out over many backbone configurations. Following Eq. (6), the exponents ν_l and ν_r are related to each other by $\nu_r = \nu_l/d_{\text{min}}$. The numerical results for ν_l and ν_r obtained by the successive slopes technique discussed in Sec. II B for regular lattices are reported in Table II. As an example, Fig. 7 shows the determination of ν_l in $d=3$.

Accordingly, the scaling variable in chemical space is l/N^{ν_l} , and the mean structural distribution function, averaged over many backbone configurations, has the form

$$\langle P_B(l, N) \rangle \propto \frac{1}{l} f(l/N^{\nu_l}) \quad (11)$$

with the scaling function

$$f_l(x) \propto \begin{cases} x^{g_l^I + d_l^B}, & x \ll 1 \\ x^{g_l^I + d_l^B} \exp(-c_{d,l} x^{\delta_l}), & x \gg 1. \end{cases} \quad (12)$$

TABLE II. Structural parameters for SAWs on the backbone of percolation clusters at criticality in $d=2$ and $d=3$, on the square and simple cubic lattice, respectively. The values for ν_r , obtained directly from the numerical data, are in agreement with the more precise values obtained from the relation $\nu_r = \nu_l/d_{\min}$. The values for $g_1^r = g_1^l d_{\min}$ are also in good agreement with the corresponding values obtained directly from the data. The numerical values for the exponents g_2^l and g_2^r have been determined using the procedure described in Appendix A. Note that there is no simple relation between g_2^l and g_2^r ; i.e., $g_2^r \neq g_2^l d_{\min}$. The values of δ_l and δ_r are consistent, within the present accuracy, with the expressions $\delta_l = 1/(1 - \nu_l)$ and $\delta_r = 1/(1 - \nu_r)$.

	$d=2$	$d=3$
γ_1	1.34 ± 0.05	1.29 ± 0.05
γ_0	1.26 ± 0.05	1.19 ± 0.05
μ_1	1.565 ± 0.005	1.462 ± 0.005
μ_0	1.456 ± 0.005	1.317 ± 0.005
ν_l	0.89 ± 0.01	0.910 ± 0.005
ν_r (directly from data)	0.778 ± 0.015	0.66 ± 0.01
$\nu_r = \nu_l/d_{\min}$	0.787 ± 0.010	0.662 ± 0.006
g_1^l	0.45 ± 0.10	0.66 ± 0.15
$g_1^r = g_1^l d_{\min}$	0.51 ± 0.11	0.91 ± 0.20
g_2^l	1.6 ± 0.16	1.95 ± 0.17
g_2^r	1.26 ± 0.18	2.96 ± 0.18
δ_l	9.5 ± 0.5	12 ± 0.5
δ_r	4.85 ± 0.20	3.1 ± 0.2

Equivalently, in r space, the scaling variable is r/N^{ν_r} , and one has

$$\langle P_B(r, N) \rangle \propto \frac{1}{r} f(r/N^{\nu_r}) \quad (13)$$

with

$$f_r(x) \propto \begin{cases} x^{g_1^r + d_f^B}, & x \ll 1 \\ x^{g_2^r + d_f^B} \exp(-c_{d,r} x^{\delta_r}), & x \gg 1. \end{cases} \quad (14)$$

Both distribution functions are normalized according to $\int_0^\infty dl \langle P_B(l, N) \rangle = 1$ and $\int_0^\infty dr \langle P_B(r, N) \rangle = 1$.

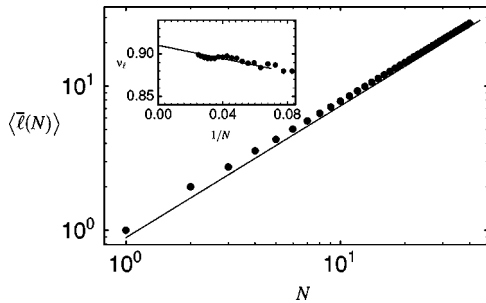


FIG. 7. The mean topological end-to-end distance $\langle \bar{l}(N) \rangle$ versus N for SAWs on the backbone of critical percolation clusters in $d=3$ averaged over 5×10^4 backbone configurations. In the inset, the successive slopes $\nu_l = d \ln \langle \bar{l}(N) \rangle / d \ln N$ are plotted versus $1/N$. A linear extrapolation of the points to the limit $1/N \rightarrow 0$ yields our estimate $\nu_l = 0.910 \pm 0.005$.

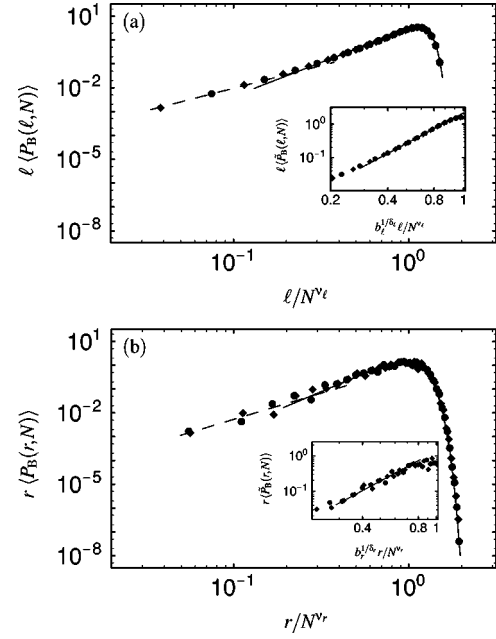


FIG. 8. Scaling plots of the distribution functions on the backbone in $d=2$, for $N=39$ and 40 , averaged over 5×10^3 configurations. (a) $l \langle P_B(l, N) \rangle$ versus l/N^{ν_l} : The dashed line has the slope 1.90 and corresponds to the ansatz Eq. (12) for $x \ll 1$; the continuous line is a fit with the ansatz Eq. (12) for $x \gg 1$, yielding $g_2^l = 1.4 \pm 0.4$, $\delta_l = 9.5 \pm 0.5$, and $c_{2,l} = 0.09 \pm 0.01$. The inset shows $l \langle \bar{P}_B(l, N) \rangle \equiv b_1^{(g_2^l + d_f^B)/\delta_l} (\Omega B_l)^{-1} l \langle P_B(l, N) \rangle \exp[(b_1^{1/\delta_l} l / N^{\nu_l})^{\delta_l}] = b_1 (l/N^{\nu_l})^{\delta_l}$ versus $b_1^{1/\delta_l} l / N^{\nu_l}$, with our estimate of the crossover value $z_l = 0.21$, according to the procedure described in Appendix A, yielding the more precise estimate $g_2^l + d_f^B = 3.05 \pm 0.15$ (continuous line). (b) $r \langle P_B(r, N) \rangle$ versus r/N^{ν_r} : The dashed line has the slope 2.15 and corresponds to the ansatz Eq. (14) for $x \ll 1$; the continuous line is a fit with the ansatz Eq. (14) for $x \gg 1$, yielding $g_2^r = 1.46 \pm 0.4$, $\delta_r = 4.9 \pm 0.3$, and $c_{2,r} = 0.79 \pm 0.10$. The inset shows $r \langle \bar{P}_B(r, N) \rangle \equiv b_r^{(g_2^r + d_f^B)/\delta_r} (\Omega B_r)^{-1} r \langle P_B(r, N) \rangle \exp[(b_r^{1/\delta_r} r / N^{\nu_r})^{\delta_r}] = b_r (r/N^{\nu_r})^{\delta_r}$ versus $b_r^{1/\delta_r} r / N^{\nu_r}$ with our estimate of the crossover value $z_r = 0.25$, according to the procedure described in Appendix A, yielding the more precise estimate $g_2^r + d_f^B = 2.9 \pm 0.15$ (continuous line).

The numerical results for the distribution functions in $d=2$ and $d=3$ are shown in Figs. 8 and 9, respectively, in both l and r space. The values for the exponents ν_l and $\nu_r = \nu_l/d_{\min}$ reported in Table II are used in the scaling variables. For the determination of the exponents g_1^l , g_2^l , g_1^r , and g_2^r according to Eqs. (12) and (14), we use the previously reported values of the fractal dimensions d_l^B and d_f^B [26]. The exponents g_1^l and g_1^r can be estimated directly from the slope of f_l and f_r in the double logarithmic plots. Since g_1^l and g_1^r are related by $g_1^r = g_1^l d_{\min}$ [15], a more precise estimate for g_1^r can be derived from the estimate for g_1^l . The determination of g_2^l and g_2^r is more difficult, since both exponents occur in the nondominant part and are masked by the exponential. Therefore it requires the use of the slightly more involved numerical procedure discussed in Appendix A (see the insets of Figs. 8 and 9 for $d=2$ and $d=3$, respectively). The numerical results we obtain for g_1^l , g_2^l , g_1^r , and g_2^r are reported in Table II. Regarding the exponential factors, our results for the exponents δ_l and δ_r are consistent,

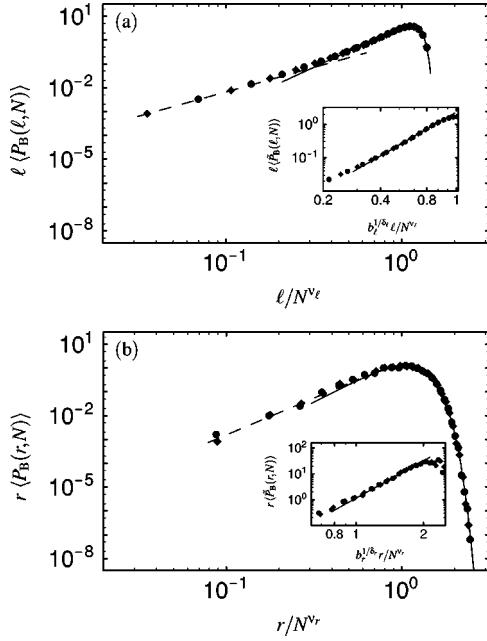


FIG. 9. Scaling plots of the distribution functions on the backbone in $d=3$, for $N=39$ and 40 , averaged over 5×10^3 configurations. (a) $l\langle P_B(l, N) \rangle$ versus l/N^{ν_l} : The dashed line has the slope 2.02 and corresponds to the ansatz Eq. (12) for $x \ll 1$; the continuous line is a fit with the ansatz Eq. (12) for $x \gg 1$, yielding $g_2^l = 1.3 \pm 0.6$, $\delta_l = 12.0 \pm 0.5$, and $c_{3,l} = 0.06 \pm 0.01$. The inset shows $l\langle \tilde{P}_B(l, N) \rangle \equiv b_l^{(g_2^l + d^B)/\delta_l} (\Omega B_l)^{-1} \langle P_B(l, N) \rangle \exp[(b_l^{1/\delta_l} l/N^{\nu_l})^{\delta_l}] = b_l (l/N^{\nu_l})^{\delta_l}$ versus $b_l^{1/\delta_l} l/N^{\nu_l}$, with our estimate of the crossover value $z_l = 0.4$, according to the procedure described in Appendix A, yielding the more precise estimate $g_2^l + d^B = 3.31 \pm 0.15$ (continuous line). (b) $r\langle P_B(r, N) \rangle$ versus r/N^{ν_r} : The dashed line has the slope 2.78 and corresponds to the ansatz Eq. (14) $x \ll 1$; the continuous line is a fit with the ansatz Eq. (14) $x \gg 1$, yielding $g_2^r = 2.3 \pm 0.6$, $\delta_r = 3.5 \pm 0.5$, and $c_{3,r} = 0.88 \pm 0.10$. The inset shows $r\langle \tilde{P}_B(r, N) \rangle \equiv b_r^{(g_2^r + d^B)/\delta_r} (\Omega B_r)^{-1} r\langle P_B(r, N) \rangle \exp[(b_r^{1/\delta_r} r/N^{\nu_r})^{\delta_r}] = b_r (r/N^{\nu_r})^{\delta_r}$ versus $b_r^{1/\delta_r} r/N^{\nu_r}$ with our estimate of the crossover value $z_r = 0.5$, yielding the more precise estimate $g_2^r + d^B = 4.83 \pm 0.15$ (continuous line).

within the present accuracy, with the expressions $\delta_l = 1/(1 - \nu_l)$ and $\delta_r = 1/(1 - \nu_r)$, respectively.

As discussed in Sec. II B, for regular lattices the exponents g_1 , ν_F , and γ are related by the des Cloizeaux relation $g_1 = (\gamma - 1)/\nu_F$. Therefore, it is legitimate to ask if a similar ‘‘generalized des Cloizeaux’’ relation holds also for SAWs in percolation. Since the enhancement exponent γ_q depends on q , it is necessary to find out whether the exponents ν_l and g_1^l as well as ν_r and g_1^r depend on q . To this end we generalize the averages $\langle \bar{l}(N) \rangle$ and $\langle \bar{r}(N) \rangle$ to $\langle \bar{l}^q(N) \rangle^{1/q} \propto N^{\nu_l^{(q)}}$ and $\langle \bar{r}^q(N) \rangle^{1/q} \propto N^{\nu_r^{(q)}}$. Since this is equivalent to studying the quantities $[\int l^q P_B(l, N) dl]^{1/q}$ and $[\int r^q P_B(r, N) dr]^{1/q}$, respectively, and $\langle P_B(l, N) \rangle$ and $\langle P_B(r, N) \rangle$ scale with l/N^{ν_l} and r/N^{ν_r} , $\langle \bar{l}^q(N) \rangle^{1/q}$ and $\langle \bar{r}^q(N) \rangle^{1/q}$ must also scale with l/N^{ν_l} and r/N^{ν_r} , respectively. Therefore $\nu_l^{(q)} = \nu_l$ and $\nu_r^{(q)} = \nu_r$ for all q , which we confirmed numerically. Furthermore, we have numerically verified that the exponents g_1^l and g_1^r (as well as g_2^l , g_2^r , δ_l , and δ_r) are independent of q . Regarding the generalized des Cloizeaux relation, our nu-

merical results suggest that in $d=2$ the relations $g_1^l = (\gamma_{q=1} - 1)/\nu_l$ and $g_1^r = (\gamma_{q=1} - 1)/\nu_r$ hold, where the to some extent arbitrary choice of $\gamma_{q=1}$ is motivated by the fact that $q=1$ describes the annealed case of the whole SAW ensemble. However, in $d=3$ these relations are not satisfied by the present numerical results.

IV. CONCLUDING REMARKS

We have studied structural properties of SAWs on the backbone of the incipient percolation cluster in both $d=2$ and $d=3$, applying exact enumeration techniques. Our results suggest that SAWs display multifractal behavior, caused by the underlying multiplicative process yielding an infinite hierarchy of generalized coordination numbers μ_q and enhancement exponents γ_q describing the moments $\langle C_{N,B}^q \rangle$ of the total number of SAWs of length N . The present results resolve previous inconsistencies regarding the suggested relation $\mu_{\text{perc}} = p_c \mu$, where p_c is the percolation threshold of a specific regular lattice, and μ and μ_{perc} are the corresponding effective coordination numbers of SAWs for the ordered case and on the incipient percolation cluster, respectively. We find that this relation is accurately obeyed on the square and simple cubic lattice by identifying $\mu_{\text{perc}} = \mu_1$.

ACKNOWLEDGMENTS

We thank A. Blumen, S. Edwards, and P. Grassberger for very useful discussions. Financial support from the German-Israeli Foundation (GIF), the Minerva Center for Mesoscopics, Fractals, and Neural Networks, and the Deutsche Forschungsgemeinschaft is gratefully acknowledged. M.P. gratefully acknowledges the Alexander von Humboldt foundation (Feodor Lynen program) for financial support.

APPENDIX A: IMPROVED PROCEDURE FOR THE DETERMINATION OF g_2

The procedure used for extracting the exponents g_2 , g_2^l , and g_2^r , describing the scaling form of the structural distribution functions, is an improved version of the procedure by Wittkop *et al.* [37] (cf. [38]) and is illustrated here for the case of regular lattices. The distribution function Eq. (4) can be written as

$$P(r, N) = \frac{\Omega B}{r} f(r/N^{\nu_F}), \quad (\text{A1})$$

with $\Omega = 2\pi$ in $d=2$ and $\Omega = 4\pi$ in $d=3$ and the scaling function $f(x)$ defined as

$$f(x) = \begin{cases} x^{g_1 + d}, & x < z \\ x^{g_2 + d} \exp(-bx^\delta), & x > z, \end{cases} \quad (\text{A2})$$

where $\delta = 1/(1 - \nu_F)$. The actual value of the crossover z is determined from the numerical results. The constants B and b can be obtained from the normalization condition

$$\int_0^\infty P(r, N) dr = 1 \quad (\text{A3})$$

and from the second moment

$$\int_0^\infty r^2 P(r, N) dr = \overline{r^2}(N) \cong N^{2\nu_F}. \quad (\text{A4})$$

Upon integration of Eqs. (A3) and (A4), one gets the exact relations

$$B = \frac{1}{\Omega} \left[\frac{1}{\delta b^{(g_2+d)/\delta}} \Gamma\left(\frac{g_2+d}{\delta}, bz^\delta\right) + \frac{z^{g_1+d}}{g_1+d} \right]^{-1}, \quad (\text{A5})$$

where $\Gamma(u, z)$ is the incomplete gamma function, and

$$\Omega B \left\{ \frac{1}{\delta b^{(g_2+d+2)/\delta}} \Gamma\left(\frac{g_2+d+2}{\delta}, bz^\delta\right) + \frac{z^{g_1+d+2}}{g_1+d+2} \right\} = 1. \quad (\text{A6})$$

Thus by plotting the distribution function in the case $x > z$ as $y \equiv b^{(g_2+d)/\delta} (\Omega B)^{-1} r P(r, N) \exp[(b^{1/\delta} r / N^{\nu_F})^\delta]$ versus $b^{1/\delta} r / N^{\nu_F}$ in a double logarithmic plot, the exponent g_2 can be read off from the relation $y \sim x^{g_2+d}$ and adjusted until the above relations Eqs. (A5) and (A6) are satisfied. This method yields much more accurate results than by directly fitting the distribution function itself. The accuracy of the result can be assessed by plotting $y \equiv -\ln[b^{(g_2+d)/\delta} (\Omega B)^{-1} r P(r, N) (b^{1/\delta} r / N^{\nu_F})^{-(g_2+d)}] = b^{(r/N^{\nu_F})^\delta}$ versus $b^{1/\delta} r / N^{\nu_F}$ in a double logarithmic plot, from which the exponent δ can be determined and compared with the expected value $\delta = 1/(1 - \nu_F)$. The procedure can be extended straightforwardly to study the distribution functions $\langle P_B(L, N) \rangle$ and $\langle P_B(r, N) \rangle$ of SAWs on the backbone of critical percolation clusters.

APPENDIX B: GENERALIZED AVERAGING PROCEDURE

To obtain an estimate of whether the ensemble \mathcal{B} of backbone configurations considered is sufficiently large to get convergent results, we analyze the data by a generalized averaging procedure as follows: The total ensemble \mathcal{B} containing n_{tot} backbone configurations is divided into subsets \mathcal{B}_i containing n_{eff} configurations each. The generalized average is then defined as

$$\langle C_{N,B} \rangle_{n_{\text{eff}}}^{(q)} = \left(\frac{1}{n_{\text{eff}}} \sum_{i=1}^{n_{\text{eff}}} (C_{N,B})_i^q \right)^{1/q}. \quad (\text{B1})$$

The obtained results $\langle C_{N,B} \rangle_{n_{\text{eff}}}^{(q)}$ depend sensitively on the dif-

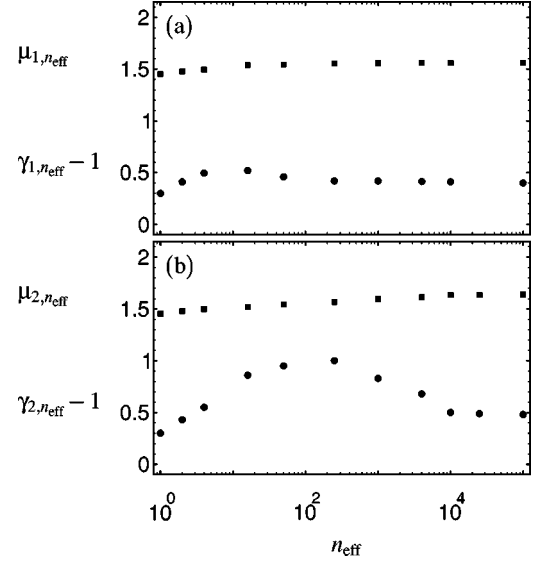


FIG. 10. The effective coordination numbers $\mu_{q,n_{\text{eff}}}$ (circles) and the enhancement exponents $\gamma_{q,n_{\text{eff}}}$ (squares) of SAWs on the backbone in $d=2$ for (a) $q=1$ and (b) $q=2$ versus the effective ensemble size n_{eff} . The values are obtained by a least-square-fit of $\{\ln[C_{N,B}(q, n_{\text{eff}})]\}/N = (\ln A_{q,n_{\text{eff}}})/N + \ln \mu_{q,n_{\text{eff}}} + [(\gamma_{q,n_{\text{eff}}} - 1) \ln N]/N$ versus N , shown as $\mu_{q,n_{\text{eff}}}$ and $\gamma_{q,n_{\text{eff}}} - 1$ versus n_{eff} .

ferent backbone configurations and display strong fluctuations, indicating that the system is not self-averaging. In order to smooth out these fluctuations, a second average is performed. This second step is a logarithmic average over the $n_{\text{tot}}/n_{\text{eff}}$ subsets [39]:

$$C_{N,B}(q, n_{\text{eff}}) = \exp\langle \ln \langle C_{N,B} \rangle_{n_{\text{eff}}}^{(q)} \rangle = A_{q,n_{\text{eff}}} \mu_{q,n_{\text{eff}}}^N N^{\gamma_{q,n_{\text{eff}}} - 1}. \quad (\text{B2})$$

In Eq. (B2), the limiting case $n_{\text{eff}}=1$ corresponds to the limit $q \rightarrow 0$, while the usual average [cf. Eq. (7)] is recovered when $n_{\text{eff}}=n_{\text{tot}}$. The results for the coordination numbers $\mu_{q,n_{\text{eff}}}$ and enhancement exponents $\gamma_{q,n_{\text{eff}}}$ are shown in Figs. 10(a) (for $q=1$) and 10(b) (for $q=2$). A dependence of these two values on n_{eff} indicates that the given ensemble is too small to obtain the asymptotic values. If, on the contrary, the ensemble of backbone configurations is sufficiently large, then $\mu_{q,n_{\text{eff}}}$ and $\gamma_{q,n_{\text{eff}}}$ no longer depend on n_{eff} . For $q=1$, this seems to be the case when $n_{\text{eff}} \gtrsim 10^3$, and for $q=2$ when $n_{\text{eff}} \gtrsim 10^4$.

[1] M. Doi and S. F. Edwards, *The Theory of Polymers Dynamics* (Clarendon, Oxford, 1986).
 [2] F. A. L. Dullien, *Porous Media, Fluid Transport and Pore Structure* (Academic, New York, 1979).
 [3] A. T. Andrews, *Electrophoresis: Clinical Applications* (Oxford University Press, New York, 1986).
 [4] A. Baumgärtner, Habilitationsschrift, Gesamthochschule Duisburg, 1995 (unpublished).
 [5] P. J. Flory, J. Am. Chem. Soc. **63**, 3083 (1941); **63**, 3091 (1941); **63**, 3096 (1941).

[6] D. Stauffer and A. Aharony, *Introduction to Percolation Theory* (Taylor & Francis, London, 1992).
 [7] M. Sahimi, *Applications of Percolation Theory* (Taylor & Francis, London, 1994).
 [8] *Fractals and Disordered Systems*, 2nd ed., edited by A. Bunde and S. Havlin (Springer, Heidelberg, 1996).
 [9] P. J. Flory, J. Chem. Phys. **17**, 303 (1949).
 [10] M. E. Fisher, J. Chem. Phys. **44**, 616 (1966).
 [11] P. G. de Gennes, *Scaling Concepts in Polymer Physics* (Cornell University Press, Ithaca, 1979).

- [12] J. des Cloizeaux and G. Jannink, *Polymers in Solution: Their Modelling and Structure* (Clarendon, Oxford, 1990).
- [13] H. Nakanishi, in *Annual Reviews of Computer Physics*, edited by D. Stauffer (World Scientific, Singapore, 1994).
- [14] K. Barat and B. K. Chakrabarti, *Phys. Rep.* **258**, 377 (1995).
- [15] H. E. Roman, J. Dräger, A. Bunde, S. Havlin, and D. Stauffer, *Phys. Rev. E* **52**, 6303 (1995).
- [16] H. E. Roman, A. Ordemann, M. Porto, A. Bunde, and S. Havlin, *Philos. Mag. B* **77**, 1357 (1998).
- [17] A. R. Conway and A. J. Guttmann, *Phys. Rev. Lett.* **77**, 5284 (1996).
- [18] B. Nienhuis, *Phys. Rev. Lett.* **49**, 1062 (1982).
- [19] A. J. Guttmann and J. Wang, *J. Phys. A* **24**, 3107 (1991).
- [20] B. Masand, U. Wilensky, J. P. Massar, and S. Redner, *J. Phys. A* **25**, L365 (1992).
- [21] J. des Cloizeaux, *Phys. Rev. A* **10**, 1665 (1974).
- [22] D. McKennzie and M. Moore, *J. Phys. A* **4**, L82 (1971).
- [23] P. L. Leath, *Phys. Rev. B* **14**, 5046 (1976).
- [24] Z. Alexandrowics, *Phys. Lett.* **A80**, 284 (1980).
- [25] H. J. Herrmann, D. C. Hong, and H. E. Stanley, *J. Phys. A* **17**, L261 (1984).
- [26] M. Porto, A. Bunde, S. Havlin, and H. E. Roman, *Phys. Rev. E* **56**, 1667 (1997).
- [27] R. Pike and H. E. Stanley, *J. Phys. A* **14**, L169 (1981).
- [28] S. Havlin and D. Ben-Avraham, *Adv. Phys.* **36**, 695 (1987).
- [29] P. Grassberger, *J. Phys. A* **32**, 6233 (1999).
- [30] P. Grassberger, *J. Phys. A* **26**, 1023 (1993).
- [31] A. Giacometti and A. Maritan, *Phys. Rev. E* **49**, 227 (1994).
- [32] P. M. Lam, *J. Phys. A* **23**, L831 (1990).
- [33] H. Nakanishi and S. B. Lee, *J. Phys. A* **24**, 1355 (1991).
- [34] K. Y. Woo and S. B. Lee, *Phys. Rev. A* **44**, 999 (1991).
- [35] R. M. Ziff, *Phys. Rev. Lett.* **72**, 1942 (1994).
- [36] P. Grassberger, *J. Phys. A* **25**, 5867 (1992).
- [37] M. Wittkop, S. Kreitmeier, and D. Göritz, *J. Chem. Phys.* **104**, 351 (1996).
- [38] R. Everaers, I. S. Graham, and M. J. Zuckermann, *J. Phys. A* **28**, 1271 (1995).
- [39] A. Bunde and J. Dräger, *Phys. Rev. E* **52**, 53 (1995).